Effects of Electrode Misalignment and Flow Rate Changes on the Thrust in an Electron Bombardment Engine

G. R. NUDD* AND K. AMBOSS†
Hughes Research Laboratories, Malibu, Calif.

The effects of electrode misalignment and ion current variations on the thrust from a single aperture of an electron bombardment ion engine have been investigated using a digital computer. Four types of perturbation have been considered: changes in ion emission rate, changes in axial spacing of the electrodes, transverse misalignment, and tilt between the electrodes. The positions of the plasma boundaries have been determined self consistently with the ion flow rate and electrode configuration for each case. A first-order analysis of the effects of perturbations that destroy the symmetry of the flow has been formed by a suitable combination of solutions obtained assuming planar and circular symmetry. It has been shown that the axial thrust varies linearly with moderate changes in the ion flow rate. Axial changes in electrode spacing produce thrust changes that depend on the operating level and are higher at the higher flow rates. For transverse displacements the changes in ion flow rate as a result of plasma sheath movements are negligible, and the change in thrust results primarily from the geometric changes of the trajectories. It has also been shown that for tilts of the magnitude likely to be encountered, the changes in the thrust are negligible.

I. Introduction

ELECTRICALLY propelled spacecraft appear to offer the most practical and effective means of exploration for long interplanetary missions. This is partly due to the ion propulsion engine's capability of efficiently producing low-level thrust for extremely long periods. With this capability comes the requirement of knowing accurately the magnitude and direction of the thrust vector produced.

The most promising ion engine for extended missions is the electron bombardment engine shown schematically in Fig. 1. A neutral plasma is generated in the discharge chamber; ions from it are extracted through the round holes of the multiapertured screen electrode and are accelerated out of the spacecraft through a similarly perforated electrode. They are then mixed with electrons to form a plasma again, in order to preserve the neutrality of the vehicle.

The plasma regions are contained by a thin sheath, the contours of which determine the ion flow and hence the thrust direction. Figure 2 shows the plasma boundaries and the ion flow in a diametral plane through one such pair of apertures.

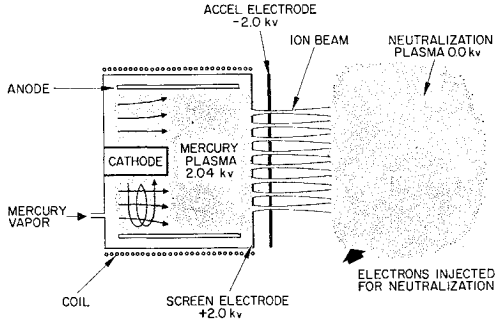

Fig. 1 Schematic of electron bombardment engine.

The positions of the sheaths are determined by the propellant flow rate and the applied fields. Changes in these quantities cause the sheaths to take up new equilibrium positions and thus lead to differences in ion flows and thrusts. Because of the high temperatures produced in the discharge chamber the relatively thin and closely spaced electrodes may become misaligned, and such field changes are thus quite possible. This paper is concerned with the effect which misalignments such as those shown in Fig. 3 may have on the thrust.

The problem of locating the plasma boundaries has received some attention in the literature. Seitz and Eilenberg[1] have used a digital computer to locate the downstream boundary for the case in which ions are generated by contact ionization at a fixed surface. Kramer and King[2] have used an electrolytic tank with space charge injection to determine the location of the upstream plasma boundary in order to calculate the ion flow through a pair of apertures of an electron bombardment thruster. In their studies the ion flow variation across the sheath was assumed and the downstream boundary was considered fixed.

Similar calculations for the geometry of a duo-plasmatron type of ion source were carried out by Harrison[3] with a uniform extraction current and a planar termination of the flow downstream.

Lathem[4] has studied on a digital computer the flow through a pair of misaligned apertures. The problem was simplified by considering that the geometry was planar and by maintaining the upstream plasma boundary in its unperturbed position under all circumstances. The downstream termination of the flow was a planar equipotential at an assumed position. The results of Lathem's study are in qualitative agree-

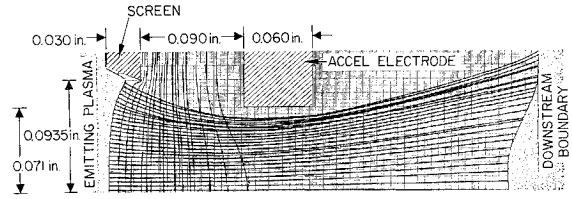

Fig. 2 Plasma boundaries and beam profile for the unperturbed engine configuration.

Received April 25, 1969; revision received October 15, 1969.

* Member of the Technical Staff, Electron Device Physics Department.

† Head, Electron Guns and Beams Section, Electron Device Physics Department; now Independent Consultant.

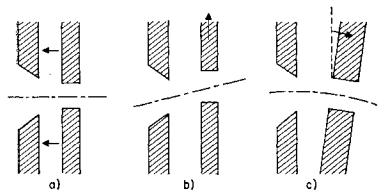

Fig. 3 Basic electrode misalignments.

ment with a tolerance study by Amboss[5] on conical flow Pierce guns with similar flow properties.

Recently Pawlik et al.,[6] used the electrostatic tank and analog computer to study the flow from an electron bombardment thruster. However, to our knowledge, no prior attempt has been made to determine self-consistently both the upstream and downstream boundary with the accuracy of the digital computer. Since the geometric perturbations are relatively small, small changes are involved and it was believed that an accurate self-consistent solution should be obtained; for this reason the problem was solved on the digital computer rather than with the electrolytic tank, and effects neglected by previous workers were considered. The computer program used is a modification of one written by Hamza and Richley[7] and is capable of calculating self-consistent space charge flows of axial and planar symmetry. Problems involving azimuthal departures from axial symmetry cannot be solved directly; in the present problem, which involves only small departures from axial symmetry, a solution was obtained by superposition of a planar on the axisymmetric solution.

The model chosen for the analysis and the simplifications imposed by the computer program are presented in Sec. II. No attempt is made to discuss the program itself since it is described fully by Harrison.[3]

Section III deals with the effect of perturbations of the electron bombardment thruster geometry that do not destroy the rotational symmetry of the electrodes and the effect of changes in the propellant arrival rate.

Section IV describes the method used to analyze transverse electrode motions and gives the results obtained for such misalignments.

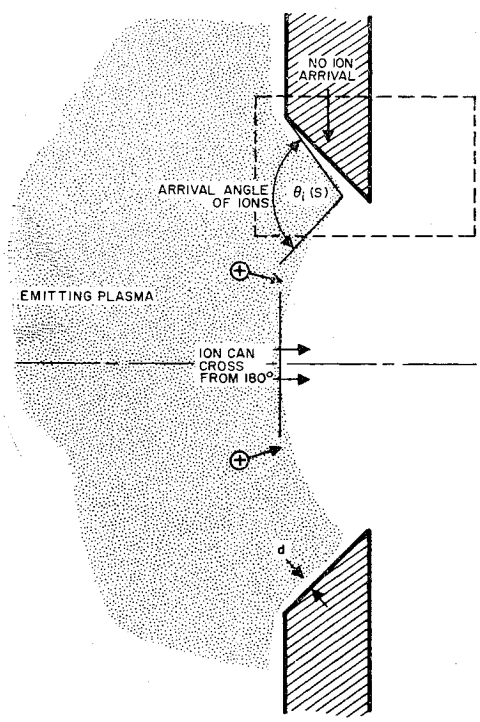

Fig. 4 Geometry of the sheath at the emitter showing the shielding effect of the screen.

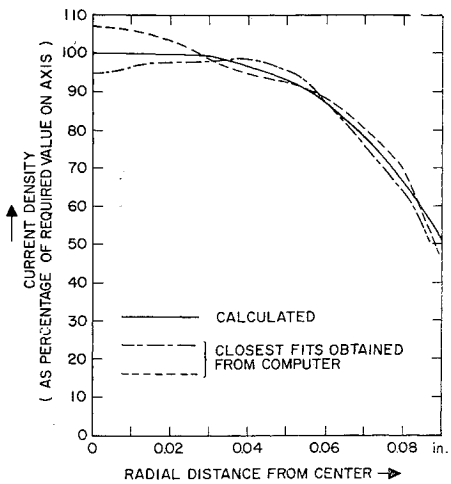

Fig. 5 The current density variation across the unperturbed sheath calculated from the arrival angle compared with the two closest variations obtained from the computer.

II. Analytical Model and the Computational Technique

The neutral plasma of the electron bombardment engine is generated by ionizing collisions with electrons which enter one end of the discharge chamber with an energy of about 40 ev. For efficient utilization the electrons are constrained by a weak magnetic field as in a Penning discharge in order to make multiple collisions. Probing of the plasma[8] shows that it is very nearly at a uniform potential of 40 v with respect to the surrounding walls, but with a radial variation in density such that the density on the chamber axis is about four times that at the edges. The peak plasma density is of the order of 10^{11} ions/cm^3 and the ion temperature is 300°C; the mean free path of an ion is therefore about 10 cm. The arrival of ions at any specified position on the screen is therefore anisotropic. This effect has not been taken into account in our analytic model; on the other hand, the reduction in arrival rate at positions on the sheath as a result of shielding by the screen electrode and by the plasma sheath itself is considered in the following manner. Since the mean free path is long compared with the screen thickness, the ion paths can be assumed to be collision free in the vicinity of the screen electrode and the ion arrival rate at a point on the emitting surface can be calculated from the solid angle subtended there. Figure 4 shows the angle $\theta(s)$ in a diametral plane. If $\psi(s)$ is the corresponding angle in a plane normal to that shown in Fig. 4, the local current density $J(s)$ is proportional to the product of the angles $\theta(s)$ and $\psi(s)$. For the sheath position shown in Fig. 2 the radial current density variation is as shown in Fig. 5.

The position of the sheath of course is not known a priori, but it must be compatible with the boundary conditions appropriate to the plasma-beam interface.[8] These are the following: 1) the plasma sheath must be an equipotential surface, 2) the normal derivative of the voltage at the sheath must be zero, and 3) the ion flow at each point across the surface must be equal to the ion arrival rate.

Elsewhere within the region of pure ion flow, Poisson's equation $\nabla^2\Phi = -\rho/\epsilon_0$ and the trajectory equation must be satisfied self-consistently. Laplace's equation $\nabla^2\Phi = 0$ must be satisfied in the region outside the flow.

The problem involves the location of two free boundaries: the upstream sheath and the downstream sheath. Because the computer programs will provide solutions to Laplace's and Poisson's equation only in the interior of closed regions, it is necessary to specify a priori a trial sheath contour and to compare the solution obtained for this surface with restric-

tions imposed on it by the aforementioned boundary conditions.

The condition that the sheath must be an equipotential surface is easily satisfied by imposing this restriction on the part of the boundary curve which represents the sheath. The condition of zero normal electric field is satisfied automatically by the computer program for the emitting portion of the trial boundary since the flow which this program calculates is from a space charge limited emitter. However, the zero normal field condition is not satisfied at the downstream boundary and must be found by systematic successive displacement of the trial boundary (e.g., in the manner outlined by Seitz and Eilenberg[1]).

Matching of the variation in ion flow is accomplished in the same manner by translation of the upstream trial boundary. However, this boundary condition is most difficult to satisfy because small local displacements affect the space charge distribution not only in its immediate vicinity, but also at considerable distances from this perturbation along the sheath. This makes an exact match virtually impossible. This computational space charge instability is only partially associated with the use of finite difference methods.[9] It is primarily a reflection of conditions that exist in nature because the space charge cloud in front of even stationary emitters is never quiescent. The effect has received considerable attention in the literature[10-12] for the case of the electron cloud in front of thermionic emitters because noise in electron devices is a direct result of space charge fluctuations near the emitter.

In the plasma boundary it is to be expected that a stationary sheath does not even exist. In the present calculations the upstream sheath position used is an average of the two closest locations which bracket the desired ion flow profile. However, the ion flow profile for the sheath position used in subsequent calculations is not that calculated by the program, but is the value imposed by the boundary conditions.

Because the emitting plasma is at approximately +40 v with respect to the screen electrode, the plasma surface is not attached to the screen electrode but lies approximately parallel to it at a distance d. As a first approximation d can be calculated from Child's[13] law for space charge flow between parallel plates with an appropriate uniform emission density. In the region near the top of the screen electrode where the plasma sheath turns away from the electrode (see Fig. 2), the surfaces are no longer parallel since the angle of ion arrival changes rapidly and this simple calculation breaks down. Previous workers have neglected this region in their analyses because it is difficult to obtain a self-consistent solution. In the present effort this corner effect was studied in the manner described below, and conditions were found under which it could be excluded from the calculations.

A self-consistent calculation was first made in which the plasma sheath was terminated on the screen electrode. The region in the vicinity of the corner, encompassed by the dotted line in Fig. 4, was then re-examined with a much finer mesh. For appropriate parts of the boundary, the potentials generated by the previous calculation were used and the plasma sheath was terminated at a distance d from the electrode. The curvature of the sheath was then established as outlined previously. Figure 6 shows the flow in that region. The ions impinging on the screen electrode are of no interest, of course, and hence it is seen the major portion of the bend in the plasma sheath can be excluded from the region of analysis. The computer program starts ions normal to the plasma surface; the sheath is therefore conveniently terminated by the ion trajectory which grazes the tip of the screen electrode.

A further simplification proved to be possible. The space charge density in the vicinity of the downstream plasma was found to be sufficiently low that small changes in the charge distribution there, as a result of upstream perturbations, had a negligible effect. Hence it proved possible to use, with negligible error, the same downstream boundary for all calculations.

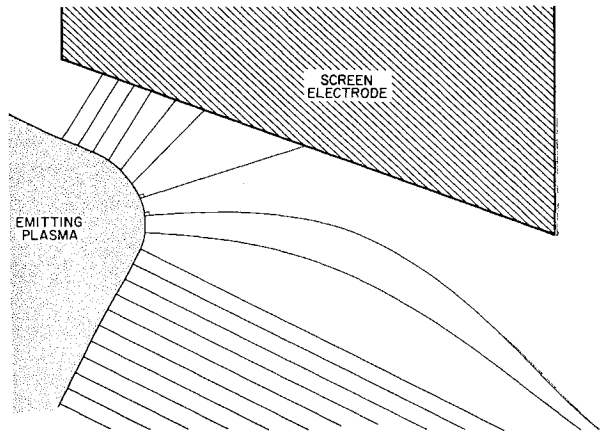

Fig. 6 Ion flow in the vicinity of the screen electrode.

III. Effect of Axially Symmetric Perturbations

The possible perturbations consist of an axial movement of the electrode illustrated in Fig. 3a or a change in flow rate; the latter effect can be simulated by a change in voltage. Since the rotational symmetry is preserved, only the axial thrust is affected for an individual pair of apertures. However, when these are summed over all of the holes of the engine with a range of spacings, a couple may result, tending to rotate the engine.

When used to solve problems with axial symmetry, the digital computer program divides the flow into 13 annular beamlets centered on the axis of the system and calculates a self-consistent ion trajectory for each beamlet. Each trajectory so calculated illustrates the flow of all ions emitted from an annular segment of the emitting sheath.

If I_i is the current associated with the ith annular segment, the total axial thrust T_A from a pair of apertures is given by

$$T_A = k \sum_{i=1}^{13} I_i(\Phi)^{1/2} \cos\phi_i \tag{1}$$

where the summation is for all segments and where $\Phi \equiv$ voltage difference between upstream and downstream plasmas, $\phi_i \equiv$ angle between trajectory and axis at downstream boundary (the exit angle), $k \equiv$ const.

The transverse thrust $T_\perp$ is given by an expression similar to Eq. (1) and is

$$T_\perp = \sum_{i=1}^{13} I_i(\Phi)^{1/2} \sin\phi_i \tag{2}$$

Because of axial symmetry, however, the summation leads to zero.

It has been found that the major contribution to the change in thrust for axial displacements results from the movement of the upstream plasma boundary rather than from the change of direction of the trajectories downstream. A change in screen-accel electrode spacing causes the form and position of the boundary to change, resulting in a change in emitting area and hence in the total emitted current. The total current I_t passing through a single aperture in the screen electrode can be expressed as

$$I_t = j_0 \sum^{As} (\Delta A_i) F_i \tag{3}$$

Here j_0 is the unobstructed arrival density at the plasma sheath, (ΔA_i) is the element of area associated with the ith trajectory, and F_i is the "view factor" which accounts for the decrease in arrival rate due to the shielding by the screen

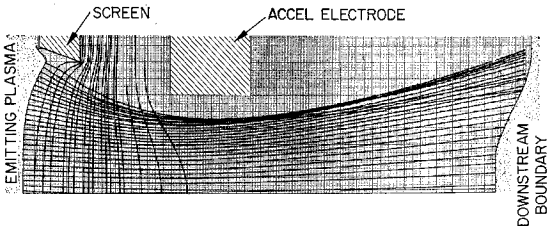

Fig. 7 Plasma boundaries and ion trajectories for the conditions of case 2 in Table 1.

electrode and by the plasma sheath. A_s is the total surface area of the emitting plasma, and the summation is for all elements on the emitting surface. It can be seen that an increase in area A_s will cause an increase in total current and hence an increase in the thrust. The axial thrust from an aperture calculated from Eq. (1) can be expressed by means of Eq. (3) as

$$T_A = k(\Phi)^{1/2} j_0 \sum_{i=1}^{13} (\Delta A_i) F_i \cos\phi_i \tag{4}$$

Changes in spacing and/or in the ion arrival rate produce a movement of the plasma sheath and result in changes in A_s, F_i, and ϕ_i; hence from Eq. (4) we find that for small changes

$$\delta T_A = \sum_{i=1}^{13} \frac{\partial T_i}{\partial(\Delta A_i)} \delta(\Delta A_i) + \sum_{i=1}^{13} \frac{\partial T_i}{\partial F_i} \delta F_i + \sum_{i=1}^{13} \frac{\partial T_i}{\partial(\cos\phi_i)} \delta(\cos\phi_i) + \sum_{i=1}^{13} \frac{\partial T_i}{\partial j_0} \delta(j_0) \tag{5}$$

where T_i is the thrust associated with the ith trajectory. Using Eq. (4), we may rewrite this expression as

$$\frac{\delta T_A}{T_A} = \frac{\delta T_{1,A}}{T_A} + \frac{\delta T_{2,A}}{T_A} + \frac{\delta T_{3,A}}{T_A} + \frac{\delta T_{4,A}}{T_A} \tag{6}$$

where

$$\delta T_{1,A} = \sum_{i=1}^{13} \frac{\partial T_i}{\partial(\cos\phi_i)} \delta(\cos\phi_i) \equiv$$

change in axial thrust due to change in ion paths alone,

$$\delta T_{2,A} = \sum_{i=1}^{13} \frac{\partial T_i}{\partial(\Delta A_i)} \delta(\Delta A_i) \equiv$$

change in axial thrust due to change in the emitting sheath area alone,

$$\delta T_{3,A} = \sum_{i=1}^{13} \frac{\partial T_i}{\partial F_i} \delta(F_i) \equiv$$

change in axial thrust due to change in view factor alone,

$$\delta T_{4,A} = \frac{\delta j_0}{j_0} \sum_{i=1}^{13} T_i \equiv$$

change in axial thrust due to change in arrival rate alone.

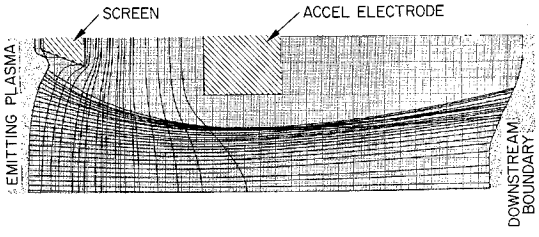

Fig. 8 Plasma boundaries and ion trajectories for the conditions of case 3 in Table 1.

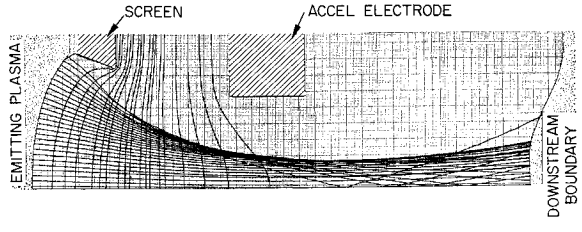

Fig. 9 Plasma boundaries and ion trajectories for the conditions of case 4 in Table 1.

The axisymmetric geometric perturbations and the changes in ion flow rate which are analyzed are listed in Table 1. Figures 2 and 7–10 are computer drawings of the corresponding profiles of the plasma sheaths and representative ion trajectories. Case 1 represents the "nominal" unperturbed case and case 2 the flow when the screen-accel electrode spacing is decreased. It is interesting to note that the total current through the aperture has increased as a result of the increase in the area of the emitting sheath, which must retreat into the plasma in order to satisfy the boundary conditions. Inspection of Table 1 shows that this effect alone is primarily responsible for the computed change in thrust.

Case 3 shows the effect of approximately halving the flow rate in the nominal geometry. Table 1 shows that the reduction in flow rate was not exactly 50%; the discrepancy is caused by the changes in sheath position and view factor, which make it difficult to calculate precisely a desired reduction in flow.

Case 4 deals with a further decrease in flow rate to about one-quarter of the nominal value, and case 5 shows the effect of a subsequent decrease in electrode spacing. As Table 1 shows, the axial thrust is most affected by the change in the ion flow due to the change in area of the sheath; it is affected to a much lesser extent by any perturbation to the trajectories.

IV. Effect of Transverse Misalignment

When a transverse misalignment of the accel electrode is made, as illustrated in Fig. 3b, the rotational symmetry of the system is destroyed and the problem cannot be analyzed directly. However, when the displacement is small a first-order approximation can be obtained by a combination of a perturbed planar solution and an unperturbed axially symmetric solution.

The method of approach is as follows: the unperturbed geometry is first analyzed self-consistently as an axially symmetric problem and then run with the same sheath configuration as a planar problem. Next the planar problem is analyzed self-consistently with the desired transverse displacement of the electrode. For each planar ion trajectory the resulting difference in path and exit angles must then be added to the equivalent axially symmetric trajectory with a suitable azimuthal dependence in order to find the perturbed solution.

Figure 11 illustrates the path difference between the unperturbed axially symmetric and planar solutions. It can

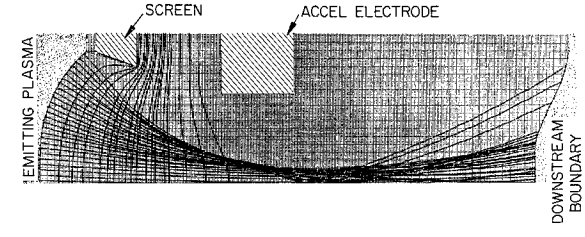

Fig. 10 Plasma boundaries and ion trajectories for the conditions of case 5 in Table 1.

Table 1 Changes in thrust for perturbations that preserve axial symmetry

Case number	Screen-accel spacing, in.	Total ion current, ma	Axial thrust, μlb	$\frac{\delta T_A}{T_A}$, %	$\frac{\delta T_{1,A}}{T_A}$, %	$\frac{\delta T_{2,A}}{T_A}$ %	$\frac{\delta T_{3,A}}{T_A}$, %	$\frac{\delta T_{4,A}}{T_A}$, %
1	0.090	1.32	25.03	...	...	...	...	...
2	0.070	1.49	28.29	13	1.43	8.9	2.67	...
3	0.090	0.753	15.02	−40	2.96	8.6	2.7	−54.3
4	0.090	0.382	8.21	...	...	...	...	...
5	0.070	0.429	8.87	8.0	3.4	4.5	0.1	...

be seen that the paths correspond over a considerable distance from the emitting sheath, so that the location of this sheath remains essentially correct.

The form of the azimuthal dependence of the perturbation is obtained from the equation of the accel hole in the displaced position. If ϵa in Fig. 12 is the displacement of its center where a is the radius of the accel hole, the radius vector R to the edge of the hole from the unperturbed axis has, to the first order in ϵ, the following variation with θ:

$$R = a[1 + \epsilon \sin\theta] \tag{7}$$

this result is readily obtained from trigonometric considerations.

If two sections are drawn through the system normal to each other, representing the planes of least and greatest perturbations, the axis lines of the two electrodes will coincide in the first plane and be displaced by ϵa in the second plane. The trajectory equation can be solved as a planar problem for these two cases, and the result will be as illustrated in Fig. 13.

For the solution of planar problems the program was arranged to divide the emitter into 26 strips and to calculate 27 trajectories, i.e., one more than is seen in a diametral plane in the axially symmetric case. The additional trajectory, number 14, corresponds to the axial trajectory which is curved in the presence of a transverse misalignment.

The effect of the transverse displacements of the trajectories can be thought of as displacing each trajectory through an exit angle δ_i; for the trajectories nearest to the electrodes the change in exit angle is $-\delta_{27}$ at the top and δ_1 at the bottom. If it is assumed that the exit angle varies as $\sin\theta$ in the azimuthal direction, as shown in Fig. 14, the angular displacement $\delta\phi'_{13}$ of the outermost trajectory in a plane at an angle $(\pi/2 - \theta)$ from the plane of the displacement can be written as

$$\delta\phi'_{13} = -\tfrac{1}{2}(\delta_{\cdot} + \delta_{27}) \sin\theta + \tfrac{1}{2}(\delta_1 - \delta_{27}) \tag{8}$$

In a plane normal to the displacement where $\theta = 0$, the change in exit angle $\delta\phi'_{13}$ is $\frac{1}{2}(\delta_1 - \delta_{27})$. In the plane of the displacement at $\theta = \pi/2$, $\delta\phi'_{13} = -\delta_{27}$; at $\theta = -\pi/2$, $\delta\phi_i = \delta_i$. Hence from a small element shown in Fig. 15, where the current density is $\bar{j}_i$, the axial thrust $\Delta T_{A,i}$ is given by

$$\Delta T_{A,i} = kR_i t_i (\Phi)^{1/2} \bar{j}_i \cos\phi'_i \delta\theta \tag{9}$$

where $R_i \equiv$ radial coordinate of the element, $\delta\theta \equiv$ angular width of the element, $t_i \equiv$ radial width of the element, $\phi'_i \equiv$ perturbed exit angle.

R_i, t_i, and $\bar{j}_i$ are functions of θ. The variation in j_i is due only to variation in the shielding effect of the screen electrode because of the asymmetry in the upstream boundary; since the sheath advances on one side of the hole and retreats on the opposite side, the integrated effect is very small (see calculation in Appendix). Similar considerations also allow us to disregard the θ dependence of R_i and t_i.

The perturbed exit angle for the ith of the axially symmetric trajectories is

$$\phi'_i = \phi_i - \left[\frac{\delta_{(14-i)} + \delta_{(14+i)}}{2}\right] \sin\theta + \left[\frac{\delta_{(14-i)} - \delta_{(14+i)}}{2}\right] \tag{10}$$

with i ranging from 1 to 13. The trajectory labeled 14 on the planar problem describes the perturbed axis of symmetry; since there is no current element associated with it, it does not contribute to the thrust.

Substitution into Eq. (9) and integration over 2π gives the following axial thrust $T_{A,i}$ associated with the ith annular

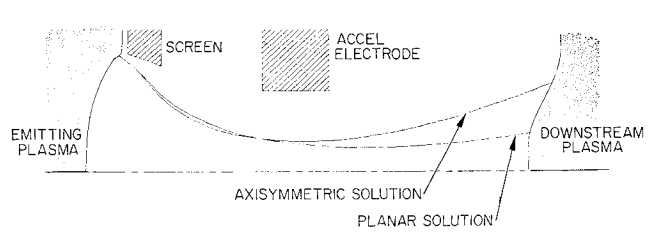

Fig. 11 Difference in ion trajectories when the same geometry is run as a planar problem and as an axially symmetric problem.

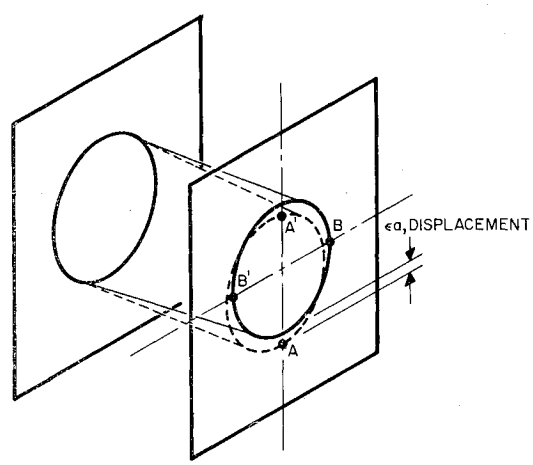

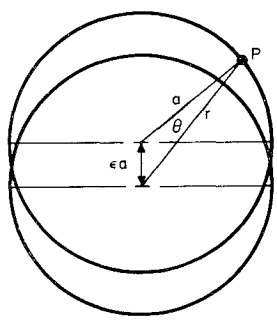

Fig. 12 Construction diagram for the transverse displacement of the accel electrode.

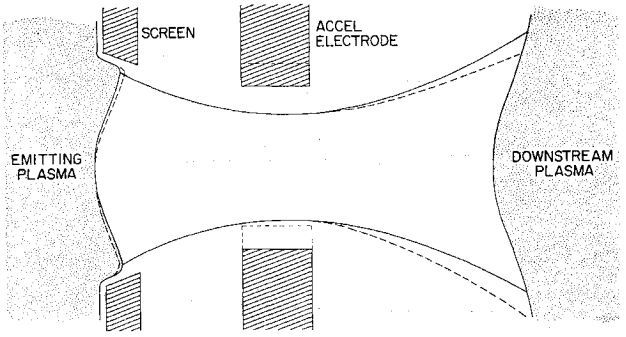

Fig. 13 Effect of translational misalignment of the ion paths calculated assuming planar symmetry (dotted lines represent the perturbed paths).

element:

$$T_{A,i} = \frac{kI_i(\Phi)^{1/2}}{2\pi}\int_0^{2\pi}\cos\left\{\phi_i - \left[\frac{\delta_{(14-i)}+\delta_{(14+i)}}{2}\right]\times \sin\theta + \left[\frac{\delta_{(14-i)}-\delta_{(14+i)}}{2}\right]\right\}d\theta \quad (11)$$

$$= kI_i(\Phi)^{1/2}J_0\left[\frac{\delta_{(14-i)}+\delta_{(14+i)}}{2}\right]\times \cos\left[\phi_i + \frac{\delta_{(14-i)}-\delta_{(14+i)}}{2}\right]$$

Here J_0 is the zero-order Bessel function and $I_i = 2\pi R_i t_i \bar{j}_i$ is again the current associated with ith annular element. The total axial thrust is therefore

$$T_A = k(\Phi)^{1/2}\sum_{i=1}^{13} I_i J_0\left[\frac{\delta_{(14-i)}+\delta_{(14+i)}}{2}\right]\times \cos\left[\phi_i + \frac{\delta_{(14-i)}-\delta_{(14+i)}}{2}\right] \quad (12)$$

The transverse thrust is a vector which can be resolved into a component parallel to the electrode displacement $T_\perp$ and a component $T_\perp{}^*$ normal to this direction. Neglecting as before second-order effects associated with the accuracy in prescribing the transverse angle, we find that

$$T_{\perp,i} = \frac{k(\Phi)^{1/2}}{2\pi} I_i \int_0^{2\pi} \sin\phi'_i \sin\theta d\theta \quad (13)$$

and

$$T_{\perp,i}{}^* = \frac{k(\Phi)^{1/2}}{2\pi} I_i \int_0^{2\pi} \sin\phi'_i \cos\theta d\theta \quad (14)$$

The latter expression, when integrated, is zero because of the odd symmetry, so that $T_i{}^* = 0$. The integral (13) is

$$T_{\perp,i} = kI_i(\Phi)^{1/2}J_1\left[\frac{\delta_{(14-i)}+\delta_{(14+i)}}{2}\right]\times \cos\left[\phi_i + \frac{\delta_{(14-i)}-\delta_{(14+i)}}{2}\right] \quad (15)$$

where J_1 is the first-order Bessel function. The total transverse thrust is therefore

$$T_\perp = k(\Phi)^{1/2}\sum_{i=1}^{13} I_i J_1\left[\frac{\delta_{(14-i)}+\delta_{(14+i)}}{2}\right]\times \cos\left[\phi_i + \frac{\delta_{(14-i)}-\delta_{(14+i)}}{2}\right] \quad (16)$$

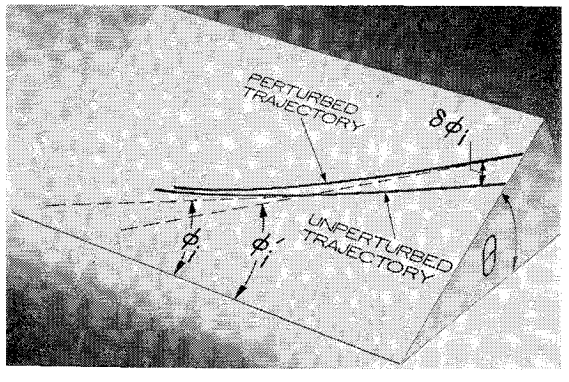

Fig. 14 Three-dimensional representation of the perturbed and unperturbed thrust.

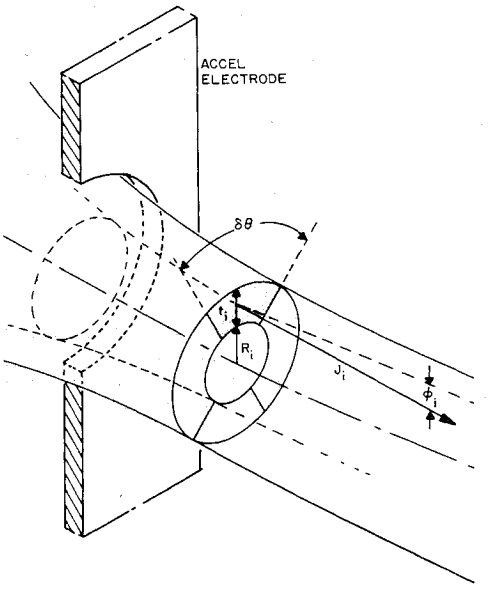

Fig. 15 Element of flow from a single aperture.

The self-consistent ion trajectories have been solved for the unperturbed and perturbed geometries, assuming planar symmetry, for two values of arrival rate corresponding to the axially symmetric cases 1 and 4. The electrode perturbations introduced were transverse displacements of the accel electrode of 0.0071 in. and 0.0142 in. The results are summarized in Table 2, and Figs. 16–19 show the computed flows. A self-consistent boundary was found in each case.

Inspection of Table 2 shows that for the ranges of displacement considered, the change in the transverse trust component is a linear function of the transverse displacement of the accel electrode. Inspection of the figures shows that the beam is deflected in the opposite direction from the electrode displacement and that the two beam edges are moved in this direction by approximately equal amounts,

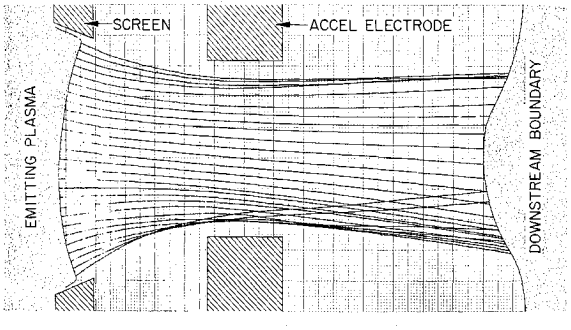

Fig. 16 Plasma boundaries and ion trajectories for the conditions of case 6 in Table 2.

Table 2 Changes in thrust due to transverse movement of the accel electrode

Case number	Screen-accel spacing, in.	Total ion current, ma	Transverse displacement of accel, in.	$\overline{\delta\phi_i}$ Average deflection, deg	Axial thrust, lb $\times 10^{-6}$	Transverse thrust, lb $\times 10^{-6}$	Rotation of thrust vector, deg
6	0.090	1.34	0.0071	4.13	24.87	1.278	2.94
7	0.090	1.35	0.0142	8.20	24.72	2.529	5.84
8	0.090	0.388	0.0071	4.49	8.12	0.357	2.52
9	0.090	0.391	0.0142	8.80	8.03	0.708	5.04

so that the factor $\delta_i - \delta_{(28-i)}$ is small. This results in agreement with previous work.[4,5]

For a typical engine with a diameter of 12 in. and a nominal spacing of 0.090 in. between the screen and accel electrode, the maximum angle for gross tilt is of the order of $\tan^{-1}$ 0.015, assuming that the electrodes are touching at the center and spaced 0.090 in. at the edges. This is equivalent to an angle of about 0.8°. (However, localized warping could increase the angle to some extent.) A case has been run with symmetric tilt of 1.5° about the unperturbed center line. This produces a maximum displacement of 0.002 in. of the accel electrode. The results from this run show no significant change in ion optics or emission density. This is in general agreement with the other reported work,[4,5] where it was found that no meaningful results could be obtained for tilt angles less than 5°.

However, tilt may be significant at the center of the engine, where the displacement of the accel electrode can be regarded as a combination of axial movement and tilt. In this case a satisfactory solution can be found by considering the appropriate axial displacement alone.

V. Conclusions

The effects of geometric perturbations and flow rate changes have been calculated for the geometry of a typical electron bombardment ion engine. The self-consistent calculations were conducted on a digital computer.

Four types of perturbation have been considered: changes in ion emission rate, changes in axial spacing of the electrodes, transverse misalignment, and tilt between the electrodes.

Changes in ion flow rate produce a nearly comparable percentage change in the axial thrust. Axial changes in electrode spacing produce a thrust change which depends on the operating level and is higher at the higher flow rates. Here the dominating factor in causing the change in thrust is not as might be expected, associated with the geometric changes of the trajectories; it is mostly associated with the movement of the emitting plasma sheath which alters the ion current through the apertures.

In the case of transverse displacements the changes in ion flow rate as a result of sheath movement are negligible, and the change in thrust is due to the geometric changes of the trajectories. It is interesting to note that the beam deflection is in the opposite direction from the movement of the electrode.

Tilt of the electrodes, which is not accompanied by a translation of the electrodes, produces a negligible effect under conditions which are likely to be encountered.

Appendix: Effects of Azimuthal Current Variations

The asymmetry of the upstream boundary causes the current density of (9) to vary azimuthally. This may be described by $\bar{\jmath}'_i = \bar{\jmath}_i + \bar{\jmath}_{i1} \sin\theta$ where $\bar{\jmath}_i$ is the zero-order current density and $\bar{\jmath}_{i1}$ is a first-order term describing the variation in shielding effect of the screen. Equation (9) can then be written

$$(\Delta T_{A,i})' = kR_i t_i (\Phi_i)^{1/2} (\bar{\jmath}_i + \bar{\jmath}_{i1} \sin\theta) \cos\phi'_i \delta\theta$$

and Eq. (11) becomes

$$(T_{A,i})' = (T_{A,i}) + \frac{kI_i}{2\pi}\left(\frac{\bar{\jmath}_{i1}}{\bar{\jmath}_i}\right) \int \cos\phi'_i \sin\theta \delta\theta$$

$$= (T_{A,i})\left\{1 + \left(\frac{j_{i1}}{j_i}\right)\frac{J_1[(\delta_{(14-i)} - \delta_{(14+i)})/2]}{J_0[(\delta_{(14-i)} - \delta_{(14+i)})/2]} \tan\phi_i\right\} \tag{11a}$$

Equation (12) then becomes

$$T'_A = T_A\left\{1 + \sum\left(\frac{T_{A,i}}{T_A}\right)\left(\frac{j_{i1}}{j_i}\right)\frac{J_1[(\delta_{(14-i)} - \delta_{(14+i)})/2]}{J_0[(\delta_{(14-i)} - \delta_{(14+i)})/2]} \times \tan\phi_i\right\}$$

or

$$\frac{T'_A - T_A}{T_A} \leq \left(\frac{T_{Ai}}{T_A}\right)_m \cdot \left(\frac{J_1[(\delta_{14-i)} - \delta_{(14+i)})/2]}{J_0[(\delta_{(14-i)} - \delta_{(14+i)})/2]}\right)_m \times (\tan\phi'_i)_m \sum\left(\frac{j_{i1}}{j_i}\right)$$

where the subscript m indicates the maximum value. For the cases considered

$$\Sigma j_{i1}/j_i < 0.03$$

whereas the first two terms of the right-hand side are of first order. Hence $T'_A = T_A$ + third-order terms. In addition, since all cases are symmetrical about $\theta = (\pi/2)$, $T_\perp{}^* = 0$

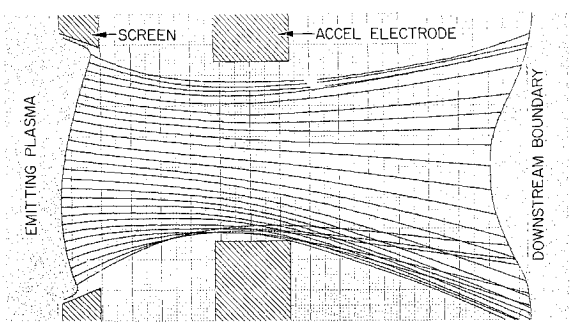

Fig. 17 Plasma boundaries and ion trajectories for the conditions of case 7 in Table 2.

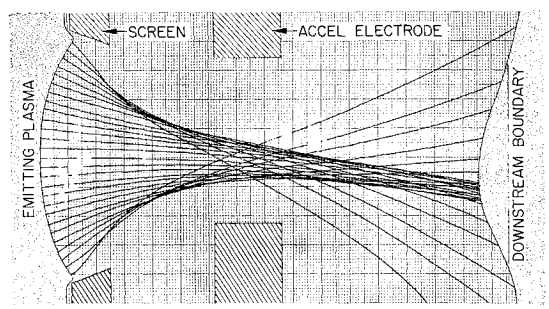

Fig. 18 Plasma boundaries and ion trajectories for the conditions of case 8 in Table 2.

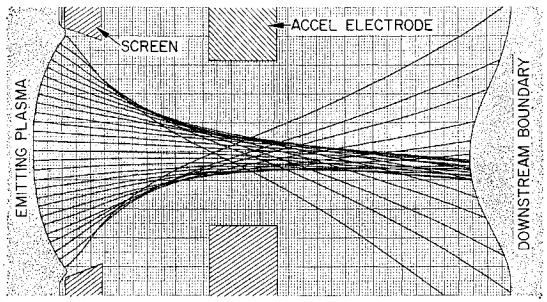

Fig. 19 Plasma boundaries and ion trajectories for the conditions of case 9 in Table 2.

throughout. However, Eq. (13) becomes

$$(T_{\perp i})' = (T_{\perp i}) + \frac{k(\Phi)^{1/2}}{2\pi} I_i \left(\frac{j_{i1}}{j_i}\right) \int_0^{2\pi} \sin\phi'_i \sin 2\theta \, d\theta \doteq$$

$$(T_{\perp i})\left\{1 + \frac{1}{2}\left(\frac{j_{i1}}{j_i}\right)\frac{J_0[(\delta_{(14-i)} + \delta_{(14+i)})/2]}{J_1[(\delta_{(14-i)} + \delta_{(14+i)})/2]}\right\} \quad (13a)$$

and

$$T'_\perp \doteq T_\perp\left[1 + \Sigma\left(\frac{T_{\perp i}}{T_\perp}\right)\left(\frac{j_{i1}}{j_i}\right)\frac{J_0[(\delta_{(14-i)} + \delta_{(14+i)})/2]}{J_1[(\delta_{(14-i)} + \delta_{(14+i)})/2]}\right]$$

or

$$\frac{T'_\perp - T_-}{T_\perp} \leq \left(\frac{T_{\perp i}}{T_\perp}\right)_m \cdot \left(\frac{J_0[(\delta_{(14-i)} + \delta_{(14+i)})/2]}{J_1[(\delta_{(14-i)} + \delta_{(14+i)})/2]}\right)_m \sum \left(\frac{j_{i1}}{j_i}\right)$$

The first two terms of the right-hand side together are of zero order, whereas

$$\Sigma(j_{i1}/j_i) \leq 0.03$$

therefore,

$$T'_\perp = T_\perp(1 + 0.03 \ldots)$$

References

[1] Seitz, W. S. and Eilenberg, S. L., "Numerical Self Consistent Field Approximation to the Interaction of an Ion Beam with a Plasma Boundary," *Journal of Applied Physics*, Vol. 38, 1967, p. 276.

[2] Kramer, N. B. and King, H., "Extraction of Dense Ion Beams from Plasmas," *Journal of Applied Physics*, Vol. 38, 1967, p. 4019.

[3] Harrison, J. L., "A Digital Computer Program for Computing Ion-Saturation Currents from a Plasma of Uniform Density in a Two-Dimensional Geometry," *Journal of Applied Physics*, Vol. 39, 1968, p. 3827.

[4] Lathem, W. C., "Effects of Electrode Misalignment in Kaufman Thrusters," *Journal of Spacecraft and Rockets*, Vol. 5, No. 6, June 1968, pp. 735–737.

[5] Amboss, K., "The Effect of Tolerances in Conical Flow Pierce Guns. I. The Perturbed Flow within the Gun," *Transactions of the IEEE*, Vol. ED-12, 1965, p. 313.

[6] Pawlik, E. V., Margosian, P. M., and Staggs, J. F., "A Technique for Obtaining Plasma-Sheath Configuration and Ion Optics for an Electron-Bombardment Ion Thruster," Rept. TND-2804, May 1965, NASA.

[7] Hamza, V. and Richley, E. A., Rept. TND-1323, 1962, NASA.

[8] Knauer, W. et al., Final Report, NASA Contract NAS 39703, 1968.

[9] Kirstein, P. T. and Hornsby, J. S., "An Investigation into the Use of Iteration Methods for the Analysis of Axially Symmetric and Sheet Beam Electrode Shapes with an Emitting Surface," *Transactions of the IEEE*, Vol. ED-11, 1964, p. 196.

[10] Lomax, R. J., "Transient Space-Charge Flow," *Journal of Electronics Control*, Vol. 9, 1960, p. 127.

[11] Bridges, W. B. and Birdsall, C. K. *Electron Dynamics of Diode Regions*, Academic Press, New York, 1966.

[12] Dunn, D. A. and Ho, I. T., "Computer Experiments on Ion-Beam Neutralization with Initially Cold Electrons," *AIAA Journal*, Vol. 1, No. 12, Dec. 1963, pp. 2770–2777.

[13] Child, C. D., "Discharge from Hot CaO," *Physical Review*, Ser. I, Vol. 32, 1911, p. 492.